Unaware processing of tools in the neural system for object-directed action representation — Source link ⌝

Marco Tettamanti, Francesca Conca, Andrea Falini, Daniela Perani

Institutions: Vita-Salute San Raffaele University

Related papers:

- The Role of Motor Action in Long-Term Memory for Objects

- Parietal maps of visual signals for bodily action planning.

- Cortical processing of object affordances for self and others' action

- Cognitive models of the perception-action cycle: A view from the brain

- Neural processes for action observation

Behavioral/Cognitive

Unaware Processing of Tools in the Neural System for Object-Directed Action Representation

⬢Marco Tettamanti,[1] ⬢Francesca Conca,[3] Andrea Falini,[2,3] and Daniela Perani[1,3]

[1]Division of Neuroscience and [2]CERMAC, Department of Neuroradiology, IRCCS San Raffaele Scientific Institute, I-20132 Milano, Italy, and [3]Vita-Salute San Raffaele University, I-20132 Milano, Italy

The hypothesis that the brain constitutively encodes observed manipulable objects for the actions they afford is still debated. Yet, crucial evidence demonstrating that, even in the absence of perceptual awareness, the mere visual appearance of a manipulable object triggers a visuomotor coding in the action representation system including the premotor cortex, has hitherto not been provided. In this fMRI study, we instantiated reliable unaware visual perception conditions by means of continuous flash suppression, and we tested in 24 healthy human participants (13 females) whether the visuomotor object-directed action representation system that includes left-hemispheric premotor, parietal, and posterior temporal cortices is activated even under subliminal perceptual conditions. We found consistent activation in the target visuomotor cortices, both with and without perceptual awareness, specifically for pictures of manipulable versus non-manipulable objects. By means of a multivariate searchlight analysis, we also found that the brain activation patterns in this visuomotor network enabled the decoding of manipulable versus non-manipulable object picture processing, both with and without awareness. These findings demonstrate the intimate neural coupling between visual perception and motor representation that underlies manipulable object processing: manipulable object stimuli specifically engage the visuomotor object-directed action representation system, in a constitutive manner that is independent from perceptual awareness. This perceptuo-motor coupling endows the brain with an efficient mechanism for monitoring and planning reactions to external stimuli in the absence of awareness.

Key words: action representation; awareness; continuous flash suppression; functional magnetic resonance imaging; object manipulation; tools

---

Significance Statement

Our brain constantly encodes the visual information that hits the retina, leading to a stimulus-specific activation of sensory and semantic representations, even for objects that we do not consciously perceive. Do these unconscious representations encompass the motor programming of actions that could be accomplished congruently with the objects' functions? In this fMRI study, we instantiated unaware visual perception conditions, by dynamically suppressing the visibility of manipulable object pictures with mondrian masks. Despite escaping conscious perception, manipulable objects activated an object-directed action representation system that includes left-hemispheric premotor, parietal, and posterior temporal cortices. This demonstrates that visuomotor encoding occurs independently of conscious object perception.

Introduction

The neural network involved in the encoding, storage, and retrieval of manipulable object knowledge comprises left-lateralized premo-

tor, parietal, and posterior temporal cortices (Johnson-Frey, 2004; Lewis, 2006; Caspers et al., 2010; Ishibashi et al., 2016). Visual perception of manipulable objects activates this visuomotor, object-directed action representation system (OAS), despite the absence of motor task requests (Chao and Martin, 2000; Grèzes et al., 2003; Canessa et al., 2008; Macdonald and Culham, 2015). A neurophysiological basis for this brain response is provided by canonical neurons, located in the ventral premotor and anterior intraparietal cortices, that fire upon visual presentation of manipulable objects (Gallese et al., 1996; Murata et al., 1997).

A controversial issue is whether visuomotor tool coding is triggered even under subliminal (Kouider and Dehaene, 2007), unaware perceptual conditions. Previous studies using continu-

Table 1. Center coordinates for small volume familywise error correction for multiple comparisons in the set of regions for tool-related cognition, as revealed by the meta-analysis of Ishibashi et al. (2016)

Brain region (Brodmann area) [area, cytoarchitectonic probability][a]	OAS	MNI coordinates, mm		
		x	y	z
L ventral premotor cortex (BA 6)	Yes	−50.3	6.3	30.7
L superior frontal gyrus/dorsal premotor cortex (BA 6)	Yes	−20.6	−4.4	62.2
L inferior parietal cortex (BA 40) [area PFt, 64%]	Yes	−45.7	−31.7	44.8
L superior parietal cortex (BA 7) [area 7A, 67%]	Yes	−23.4	−61.1	60.9
L lateral middle temporal gyrus/middle occipital gyrus (BA 19/37)	No	−47.8	−65.1	−1.8
L fusiform gyrus (BA 37) [area FG3, 83%]	No	−28.0	−46.0	−15.9
R fusiform gyrus (BA 37) [area FG3, 85%]	No	33.6	−50.5	−12.1

Our neuroanatomical predictions were targeted to the premotor and parietal regions in this set, constituting the OAS. Occipitotemporal regions, which in the same meta-analysis were identified as contributing specifically to object identification, were also tested. L, Left; R, right.

[a]Areas and cytoarchitectonic probabilities according to www.fz-juelich.de/ime/spm_anatomy_toolbox.

ous flash suppression (CFS; Tsuchiya and Koch, 2005) have found conflicting results (Ludwig and Hesselmann, 2015). A seminal fMRI study by Fang and He (2005) showed significantly reduced responses for both tool and face stimuli under CFS in the ventral visual stream, but preserved tool-specific activation in the dorsal visual stream. Behavioral picture priming experiments also provided evidence compatible with the view that suppressed tool stimuli engaged the dorsal visual stream (Almeida et al., 2008, 2010). Other fMRI studies instead reported suppressed activation in the dorsal visual stream for unawarely processed tool stimuli (Hesselmann and Malach, 2011; Hesselmann et al., 2011; Ludwig et al., 2015), as also reflected by the lack of decoding sensitivity (Fogelson et al., 2014; Ludwig et al., 2016) in a multivariate pattern analysis (MVPA). Ludwig et al. (2016) showed decodable tool versus face brain responses under CFS, though in the ventral, not in the dorsal visual stream.

A fundamental caveat of fMRI studies on unaware processing of manipulable objects so far is that they restricted their focus on posterior occipitoparietal regions, thus disregarding the essential role of the left premotor cortex, and thereby of the whole OAS as an integrated network, in manipulable object processing. Our fMRI study was specifically aimed at evaluating the recruitment of the OAS during the processing of subliminally presented pictures of manipulable objects (MOs) versus non-manipulable objects (NOs), with specific neuroanatomical predictions based on a meta-analysis on tool-related cognitive representations (Ishibashi et al., 2016). Ishibashi et al. (2016) distinguished between functions related to the planning and execution of actions directed toward tools, and functions related to tool identification. We adopted this distinction in testing the core hypothesis of our study: unaware MO processing, compared with NO processing, should specifically engage the OAS, defined as including the brain regions implicated in object-directed action processes, namely the left ventral and dorsal premotor, and the left inferior and superior parietal cortices (Table 1). Our predictions on the brain regions exclusively involved in object identification, namely the bilateral fusiform gyrus, and left occipitotemporal cortex, were instead more nuanced (i.e., either no differences, or stronger activation for NO vs MO), because there is mixed evidence with respect to the specificity of these brain regions for either tools or non-manipulable objects such as faces, animals, vehicles, and buildings (Chao et al., 1999; Ishai et al., 2000; Whatmough et al.,

2002; Saccuman et al., 2006; Wierenga et al., 2009; Bracci et al., 2012).

We determined the subjective perceptual threshold in 24 healthy human subjects, with a CFS paradigm, requiring subjective rating along a perceptual awareness scale (PAS; Ramsøy and Overgaard, 2004). During fMRI, we then used the same paradigm but with a new set of pictures reflecting manipulability (MO, NO) and contrast (5 incremental levels: 2 levels below, 1 level at perceptual threshold, 2 levels above). A null-stimulus reference baseline served as an objective control for the true absence of perception. We assessed whether the OAS specifically responded to MO following a "subliminal" activation amplitude profile, i.e., stable activation across the five incremental contrast levels, indicating unaware processing. The subliminal profile was evaluated against either a "linear" profile, i.e., activation increase with contrast, and a "step" profile, i.e., drop of activation below perceptual threshold (Fig. 1). A subliminal response in the OAS was also sought through MVPA: positive evidence would be provided by MO versus NO activation decodability both below and above perceptual threshold.

Materials and Methods

Participants. Twenty-five Italian native speakers volunteered in the experiment. One participant did not comply with the task and was discarded from the analyses. All 24 included participants (13 females, mean age 22.09 years, SD = 2.19) were right-handed (mean score 0.95, SD = 0.07) according to the Edinburgh inventory (Oldfield, 1971). Eye dominance was evaluated for the CFS task (Fig. 1A) by means of the Miles test (Miles, 1930): 4 participants were left, and 20 right eye dominant. All reported no history of neurological, psychiatric, or developmental diagnoses. They gave written consent to participate in the study after receiving a careful explanation of the procedures. The study was approved by the Ethics Committee of the San Raffaele Scientific Institute, Milano, Italy.

Experimental stimuli. We used pictures of items belonging to three different semantic categories: MOs, NOs, and living entities. MO and NO pictures were used for fMRI stimulation, living pictures for the pre-fMRI behavioral session.

All original pictures were high-resolution colored photographs, presenting a full shot of the depicted item in isolation, on a white background. The majority (85%) of pictures was drawn from the Bank of Standardized Stimuli (Brodeur et al., 2010, 2014), whereas the remaining pictures (15%) were retrieved by internet search. MO (70 pictures) included objects whose specific function is performed through manipulation with either one or both hands, such as utensils and musical instruments. NO (70 pictures) included objects whose specific function typically does not involve hand manipulation, such as buildings and seating furniture. Living entities (100 pictures) included animals and plants. The shapes of the selected pictures were roughly matched across categories for their elongation (Sakuraba et al., 2012): for instance, a violin (MO), a park bench (NO), a heron (Living); a basketball (MO), a stool (NO), a butterfly (Living).

We ran a rating study on the set of pictures to collect rating norms for visual complexity (Brodeur et al., 2014), and for two different manipulability measures (Salmon et al., 2010), that is, graspability and presence of functional motor associations. For each norming dimension, a distinct group of subjects rated all pictures on a 7-point Likert scale (1 = "low", 7 = "high"). Visual complexity (5 rating subjects: 2 females, mean age 23.75 years, SD = 0.77) resulted balanced across the three semantic categories (MO: mean = 3.73, SD = 1.06; NO: mean = 3.84, SD = 1.10; Living: mean = 3.73, SD = 0.73; Kruskal–Wallis $\chi^2_{(2)}$ = 1.103, p = 0.576). In turn, the two manipulability measures resulted unbalanced, reflecting the specificity of MO, as opposed to NO and Living items: graspability (5 rating subjects: 3 females, mean age 23.52 years, SD = 0.27; MO: mean = 6.58, SD = 0.49; NO: mean = 2.80, SD = 1.38; Living: mean = 3.13, SD = 1.10; Kruskal–Wallis $\chi_{(2)}$ = 148.948, $p < 0.001$); functional motor associations (5 rating subjects: 4 females, mean age 24.30 years, SD =
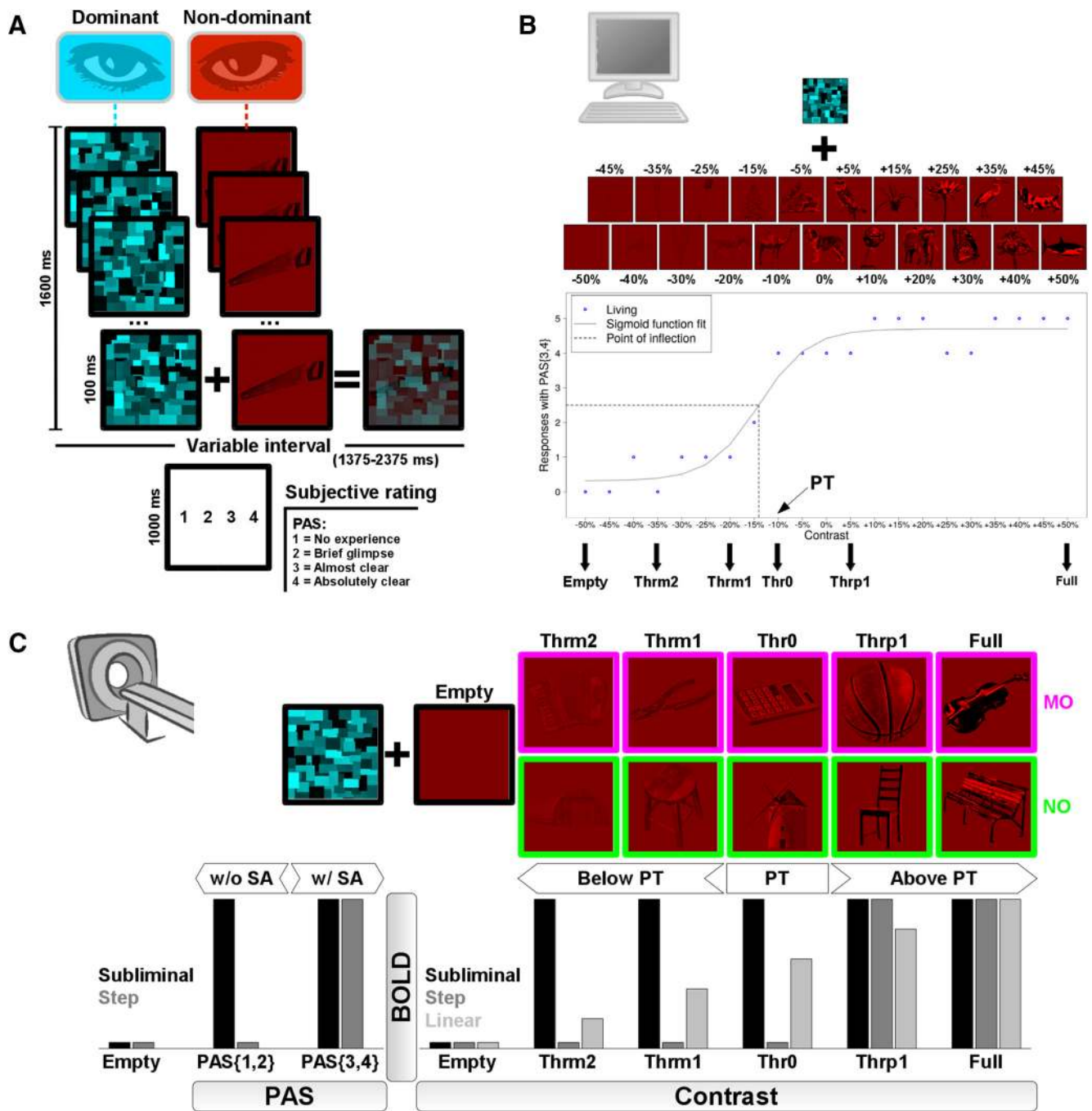
Figure 1. Experimental procedures. ***A***, A single trial of the CFS task, with the presentation of a single picture at a given contrast level, overlaid by random texture masks flickering at 10 Hz. After a short interval, the participants reported a PAS score, reflecting their stimulus' subjective awareness level. The trial structure was identical for both the behavioral and fMRI sessions. ***B***, In the pre-fMRI behavioral session, all masked stimuli belonged to the Living category. Each participant was presented with five trials for each of 21 image contrast levels, from full invisibility (−50%) to full visibility (+50%), with 5% increments. We plotted the number of responses (blue circles) with a PAS score of 3 or 4 [PAS(3,4)], indicating high to maximal subjective awareness. We then fitted a sigmoid function (see Materials and Methods), and used its point of inflection to define the subjective perceptual threshold. Six contrast levels were then set to be used in the fMRI session: a void-of-object baseline (Empty), two contrast levels below perceptual threshold (Thrm2, Thrm1), one at (Thr0), and two above (Thrp1, Full). ***C***, In the fMRI session, the masked stimuli were either MOs or NOs. We looked for MO-specific BOLD responses that fitted: (bottom right) a subliminal, as opposed to a step or linear, profile of activation as a function of contrast [i.e., activation both below and above perceptual threshold (PT)]; (bottom left) a subliminal as opposed to a step profile as a function of PAS [i.e., activation both with and without subjective awareness (SA)].

0.78; MO: mean = 6.70, SD = 0.30; NO: mean = 2.39, SD = 1.07; Living: mean = 1.80, SD = 0.54; Kruskal–Wallis $\chi^2_{(2)} = 153.882$, $p < 0.001$).

To make the stimuli suitable for the CFS task, we submitted all pictures to a customized image processing pipeline. First, all pictures were converted to black and white images, using ImageMagick 6.9 (www. imagemagick.org, RRID:SCR_014491). Second, the mean brightness value of each picture was adjusted to the overall mean brightness value calculated over the entire picture set, using MATLAB R2011a (Math-

Works, RRID:SCR_001622). Third, we increased and equalized the contrast of all pictures by means of contrast limited adaptive histogram equalization (CLAHE; Pizer et al., 1987) using Python 4.2 (www.python. org, RRID:SCR_008394). Fourth, the image contrast was normalized across the entire picture set, again using MATLAB R2011a.

With this normalized picture set, we then proceeded to generate the full gradation of image contrast levels required for our implementation of the CFS task (Fig. 1), which is based on the evidence, exploited for

instance in the breaking-CFS task variant, that stimuli with higher contrast emerge more promptly from suppression (Yang et al., 2014). For this purpose, we used GIMP 2.8 (www.gimp.org, RRID:SCR_003182) to, first, replace the white image background with gray color (RGB values: 128, 128, 128), and second, to progressively modify the object contrast by 5% incremental/decremental steps. This yielded, for each picture, a gradation of 21 different image contrast levels (Fig. 1B), ranging from −50% (i.e., full absence of object) to +50% (i.e., full visibility).

Finally, again using ImageMagick 6.9, we applied a red-channel hue to the full set of black and white images of 21 contrast levels, thus generating the final pictures that were presented to the nondominant eye during CFS (Fig. 1A).

As for the masks presented to the dominant eye, we created a texture of small rectangles of different sizes and different gray color shades, chosen to roughly match the visual characteristics of the to-be-suppressed object pictures (Yang et al., 2014). We randomized the position of the rectangles to generate 20 different mask exemplars. These were then colored with ImageMagick 6.9, by applying a cyan-channel hue (Fig. 1A).

CFS task. The CFS task was organized as a series of consecutive trials, with trial structure identical for both the pre-fMRI behavioral and fMRI sessions (Fig. 1A). In both sessions, we used Presentation 18.3 (Neurobehavioral Systems, RRID:SCR_002521) for stimulus delivery and behavioral response collection.

In each trial, a single object picture was presented for 1600 ms. During the same time interval, overlaid on this picture with 50% transparency (α blending), we presented a series of flickering masks at a frequency of 10 Hz. For each trial, 16 masks were randomly drawn, without replacement, from the pool of 20 available exemplars.

After a variable within-trial interval (randomized duration of 1375, 1875, or 2375 ms, in 4:2:1 proportion), the participants were presented for 1000 ms with the display "1 2 3 4", and had to press one among four available buttons, according to their subjective visual perception of the stimulus. Before task administration, the participants were instructed and trained (by means of a few trials with explicit feedback from the experimenters) to associate each of the four buttons with a corresponding PAS (Ramsøy and Overgaard, 2004) rating level. The four rating levels indicated increasing levels of subjective stimulus perception, from lowest to highest: 1, no experience; 2, brief glimpse; 3, almost clear image; 4, absolutely clear image. PAS scores have been found to be highly predictive of the level of performance in visual identification of subliminal stimuli (Sandberg et al., 2010), and to be concordant with objective measures of awareness (Cul et al., 2007).

We intentionally avoided questions assessing objective stimulus perception, since these could bias visual object processing, by making the focus on the object's semantic category or features explicit. Importantly, we nevertheless included a null contrast condition (void-of-object Empty baseline; Fig. 1) that constituted an objective control of absence of perception. The null contrast condition was used as a reference both in the behavioral and fMRI data analyses.

The between-trial intervals had a randomized duration of 2875, 4125, or 5125 ms (in 4:2:1 proportion).

Dichoptic stimulus view was instantiated by equipping the participants with red-cyan anaglyph plastic goggles (Carmel et al., 2010). The participants wore the cyan lens on the dominant, and the red lens on the nondominant eye, thus establishing effective suppression of the red-hue object picture.

Psychophysical assessment of perceptual threshold. In a pre-fMRI behavioral session, performed on a laptop computer (Fig. 1B), every participant was presented with 105 consecutive CFS trials. Only pictures of Living entities were included in this session, to avoid pre-exposure with MO and NO pictures underlying the fundamental neuroimaging research questions.

Presentation 18.3 was coded such that, for each participant, the 100 Living available entities were randomly ordered in a list: the entities were then sequentially taken from the list, and assigned in batches of five to 1 of 20 image contrast levels (from −45% to +50%). This effectively instantiated a draw without replacement of each item in the available pool of 100 Living pictures, with an equal number of items for each contrast level. Additionally, five stimuli with −50% contrast level (void-of-object baseline) were also taken. The total number of 105 picture stimuli were

then presented in semirandomized order, each stimulus in a separate CFS trial.

For every participant, we plotted for each of the 21 image contrast levels the number of responses (possible range: 0–5, given 5 trials × contrast) with a PAS score equal or >3 [PAS(3,4) score], indicating high to maximal subjective awareness of visual stimulus perception (Fig. 1B, blue circles). Using nonlinear least-squares estimation in MATLAB R2011a, we then fitted this PAS(3,4) score and calculated the parameters (L, R, i, W) of a psychometric sigmoid function f:

$$f = L + (R - L)/\{1 + \exp[-(x - i)/W]\},$$

where: x = Contrast level, L = left horizontal asymptote (initial value = = 0), r = right horizontal asymptote (initial value = = 5), i = point of inflection (initial value = = 2.5), and W = width of the rising interval (initial value = = 1). The estimated point of inflection i was taken as a reference for the subjective perceptual threshold, defined as the first Contrast level above the point of inflection (Fig. 1B).

fMRI experimental design. In the fMRI CFS task (Fig. 1C), only MO and NO pictures were used. We factorially manipulated the two factors Manipulability (2 levels: MO, NO) and Contrast (5 levels: Thrm2, Thrm1, Thr0, Thrp1, Full). Four levels of the Contrast factor were individually tailored for each participant, based on the estimated subjective perceptual threshold. Two of the tailored contrast levels were below threshold (Thrm2 = Threshold −25%; Thrm1 = Threshold −10%), providing subliminal stimulus presentation. One contrast level was at threshold (Thr0 = Threshold), and one was above threshold (Thrp1 = Threshold + 10%). The fifth contrast level was fixed for all participants as the maximum available contrast (Full). A null contrast control condition, namely a red square devoid of any objects, was also included for all participants (Empty). The Thrm2, Thrm1, Thr0, Thrp1, and Full contrast increments/decrements were chosen to roughly correspond to a logarithmic scale, on the basis of which we expected an approximately linear increase of PAS score responses (Ludwig et al., 2016). However, one participant had a perceptual threshold corresponding to the −35% contrast level, and the contrast levels below threshold had thus to be tailored to a narrower range (Thrm2 = Threshold − 45%; Thrm1 = Threshold − 40%). Another participant had a perceptual threshold corresponding to the +40% contrast level, and we therefore set the contrast level above threshold to a narrower range (Thrp1 = Threshold + 45%).

In the MRI scanner, the CFS task was performed in two separate fMRI acquisition runs. For this reason, the available pool of 70 MO and 70 NO pictures was equally divided in two lists, each one containing 35 MO and 35 NO pictures. Presentation 18.3 was coded in such a way that, for each fMRI run, based on a semirandomization of the list of 35 MO and 35 NO pictures that was invariant across participants, batches of 7 MO plus 7 NO pictures were drawn without replacement in sequential order and assigned to each Contrast level (Thrm2, Thrm1, Thr0, Thrp1, Full, in this exact order). Visual complexity, graspability, and functional motor associations were kept balanced across, respectively, the five batches of 7 MO and five batches of 7 NO pictures (Kruskal–Wallis $\chi^2_{(4)}$ tests, all $p > 0.17$). Additionally, seven stimuli with −50% contrast level (Empty baseline) were also taken. In this manner, all participants were presented with exactly the same depicted objects for every Contrast level, although the specific image contrast applied varied according to the individual perceptual threshold (e.g., for level Thrm1, image contrast −20% for Subject 03, and image contrast −5% for Subject 04). For each of the two fMRI runs, the selected 77 picture stimuli were then presented in semirandomized order, each one in a separate CFS trial.

Given this semirandomization procedure, and the CFS trial structure described above (CFS task section), the stimulus presentation resulted in a fMRI event-related design, with semirandomized stimulus presentation order (same randomization for all participants), and variable within-trial and between-trial intervals.

The order of the within-trial and between-trial intervals was determined by OPTseq2 (surfer.nmr.mgh.harvard.edu/optseq, RRID:SCR_014363), to maximize the hemodynamic signal sensitivity of the event-related design.

Before the experimental fMRI runs, a brief fMRI training session was administered to each participant, to verify that the participant complied to the task instructions and requests.

MRI data acquisition. Neuroimaging data were acquired on the same day of the psychophysical perceptual threshold assessment. MRI scans were acquired with a 3 Tesla Philips Achieva whole-body MR scanner (Philips Medical Systems) using an eight-channel sense head coil (sense reduction factor = 2). Whole-brain functional images were obtained with a T2*-weighted gradient-echo, EPI pulse sequence, using BOLD contrast (TR = 2000 ms, TE = 30 ms, flip angle 85°). Each functional image comprised 34 contiguous axial slices (4 mm thick), acquired in interleaved mode (field-of-view = 240 × 240 mm, matrix size = 128 × 128). Each participant underwent two consecutive functional scanning sessions, each comprising 313 scans, preceded by 5 dummy scans that were discarded before data analysis, and lasted 10 min and 36 s. A high-resolution T1-weighted anatomical scan (three-dimensional spoiled-gradient-recalled sequence, 150 slices, TR = 7.2 ms, TE = 3.5 ms, slice thickness = 1 mm, in-plane resolution 1 × 1 mm) was acquired for each participant.

The stimuli were back-projected on a screen located in front of the scanner visible to the participants through a mirror placed on the head coil above their eyes. The participants gave PAS score responses through an MRI-compatible fiber-optic response box with four buttons, using their left hand. The left hand was chosen to reduce contamination of the BOLD signal measured in the target left-hemispheric OAS. As a further mean to make this contamination negligible, the variable within-trial interval introduced a temporal lag between the visual stimulus and the button press motor response, while also reducing the temporal correlation between the two events.

Statistical analysis of behavioral data collected during fMRI. To evaluate the effects of manipulability and contrast on the PAS scores measured during fMRI, we ran a nested series of generalized linear mixed models using R 3.3.2 (R Core Team, 2016; RRID:SCR_001905). We started with the simplest model in a nested hierarchy of increasingly complex generalized linear mixed models, with PAS scores as a categorical (4-point PAS scale) dependent variable, a fixed-effect modeling the two fMRI runs, and, as random intercept effects, the participants and the picture stimuli, to account for between-subjects and between-stimuli variability. The fixed-effects predictors of PAS scores were then added stepwise to increasingly complex models. The fixed-effects predictors were manipulability (MO, NO), contrast (Thrm2, Thrm1, Thr0, Thrp1, Full), and their two-way interaction. All models were fit to a Poisson distribution and with a log-link function. Each hierarchically more complex model was tested against the hierarchically simpler model by means of a χ^2 log-likelihood ratio test (declared significance α level: 0.05) to evaluate whether there was a significant increase in model fit, and thus a significant effect of the added predictor.

Univariate statistical analysis of fMRI data. We used SPM12 v6685 (www.fil.ion.ucl.ac.uk/spm, RRID:SCR_007037) for MRI data preprocessing and univariate statistical analysis. The segment procedure was applied to the structural MRI images of each participant, with registration to the Montreal Neurological Institute (MNI) standard space. Functional images were corrected for slice timing, and spatially realigned. The images were normalized to the MNI space, using the segment procedure with the subject-specific segmented structural images as customized segmentation priors. Finally, the images were spatially smoothed with an 8 mm FWHM Gaussian kernel.

We adopted a two-stage random-effects statistical approach. The statistical analysis was restricted to an explicit mask including only the voxels with gray matter tissue probability >0.1, based on the segmented structural images of each participant.

Univariate statistical analysis of fMRI activation as a function of contrast. At the first stage, we specified a general linear model for each participant, with the time series high-pass filtered at 128 s and pre-whitened by means of an autoregressive model AR(1). No global normalization was performed. Hemodynamic evoked responses for all experimental conditions were modeled as canonical hemodynamic response functions. We modeled two separate sessions, each including 11 regressors of interest (Empty, MOThrm2, MOThrm1, MOThr0, MOThrp1, MOFull, NOThrm2, NOThrm1, NOThr0, NOThrp1, NOFull), with evoked responses aligned to the onset of each trial, and duration equal to the presentation of the masked stimuli (1600 ms). Separate regressors mod-

eled experimental confounds, including PAS score responses, aligned to the onset of the "1 2 3 4" PAS display, task instructions, and head movement realignment parameters. If present, confound regressors were also specified for miss trials, and for trials with responses given before the appearance of the "1 2 3 4" PAS display, thus eliminating trials in which an anticipated motor response may contaminate the BOLD signal evoked by masked objects. Within the estimated first-level general linear model, we defined: (1) a set of 10 condition-specific contrasts, each with a weight of +1 for the regressor-of-interest (e.g., MOThrm2) and a weight of −1 for the Empty baseline; and (2) a set of six contrasts, modeling the variation of BOLD signal with the increase of image contrast for MO and NO, according to either a subliminal, a step, or a linear BOLD amplitude model (Fig. 1C, bottom right). The contrast weights, with respect to the order of the 11 regressors of interest specified, were the following: MO subliminal: [−5 +1 +1 +1 +1 +1 0 0 0 0 0]; NO subliminal: [−5 0 0 0 0 0 +1 +1 +1 +1 +1]; MO step: [−1 −1 −1 −1 +2 +2 0 0 0 0 0]; NO step: [−1 0 0 0 0 0 −1 −1 −1 +2 +2]; MO linear: [−2.5 −1.5 −0.5 + 0.5 + 1.5 + 2.5 0 0 0 0 0]; NO linear: [−2.5 0 0 0 0 0 −1.5 −0.5 + 0.5 + 1.5 + 2.5].

Using the set of 10 condition-specific contrasts of each participant, we specified a second-level, random-effects, full factorial design. The model included the within-subjects factors manipulability and contrast (with the Empty baseline subtracted), with dependence and equal variance assumed between the levels of both factors. In this full factorial design, we investigated the main effect of manipulability, and the simple effect of manipulability for contrast levels above perceptual threshold.

Using the six contrast-to-BOLD amplitude model contrasts of each participant, we specified three second-level, random-effects, paired t test designs, investigating whether the activation differed between MO and NO as a function of image contrast level following, respectively, a subliminal, a step, or a linear distribution profile.

Univariate statistical analysis of fMRI activation as a function of PAS ratings. Contrary to the analysis of BOLD responses as a function of contrast, which rested on an equal number of CFS trials for each contrast level, the analysis as a function of PAS ratings was complicated by individual behavioral variability, with some participants markedly departing from a linear increase of PAS score with increasing contrast level (see Fig. 3), thus producing an unbalanced number of trials across the four PAS scale levels. To minimize the problem of unbalanced statistical comparisons, the analysis was restricted to only those subjects that responded with comparable frequencies across all PAS levels. This amounted to reducing the sample of participants to a subsample ($n = 12$), by estimating with R 3.3.2 the maximum likelihood of the individual Contrast-to-PAS linear function to a Contrast-to-PAS linear model function, and then by ranking the participants based on the Akaike information criterion (see Fig. 3).

For this subsample of 12 participants, we specified at the first stage a general linear model, with all parameters identical to the one modeling BOLD responses as a function of contrast, but this time reassigning the CFS trial events based on the PAS scores. This resulted in modeling five regressors-of-interest, in the following exact order: the Empty baseline (unmodified); MOPAS(1,2): all trials with MO pictures in which the reported PAS score was either 1 or 2; MOPAS(3,4): all MO trials with PAS score 3 or 4; NOPAS(1,2): all NO trials with PAS score 1 or 2; NOPAS(3,4): all NO trials with PAS score 3 or 4. Within the estimated first-level general linear model, we defined a set of four contrasts, modeling the variation of BOLD signal with the increase of PAS score for MO and NO, according to either a subliminal or a step BOLD amplitude model (Fig. 1C, bottom left). The contrast weights, with respect to the order of the five regressors-of-interest specified, were the following: MO subliminal: [−2 +1 +1 0 0]; NO subliminal: [−2 0 0 +1 +1]; MO step: [−1 −1 + 2 0 0]; NO step: [−1 0 0 −1 + 2].

Given the small sample size ($n = 12$), all second-level, random-effects analyses of BOLD activation as a function of PAS ratings were performed using nonparametric statistics, by means of the SnPM13 toolbox (Nichols and Holmes, 2002; RRID:SCR_002092). For each small volume-of-interest (6-mm-radius spheres centered on the coordinates indicated in Table 1), we specified a set of two paired t test models, investigating whether the activation differed between MO and NO as a function of PAS score following, respectively, a subliminal or a step distribution profile.
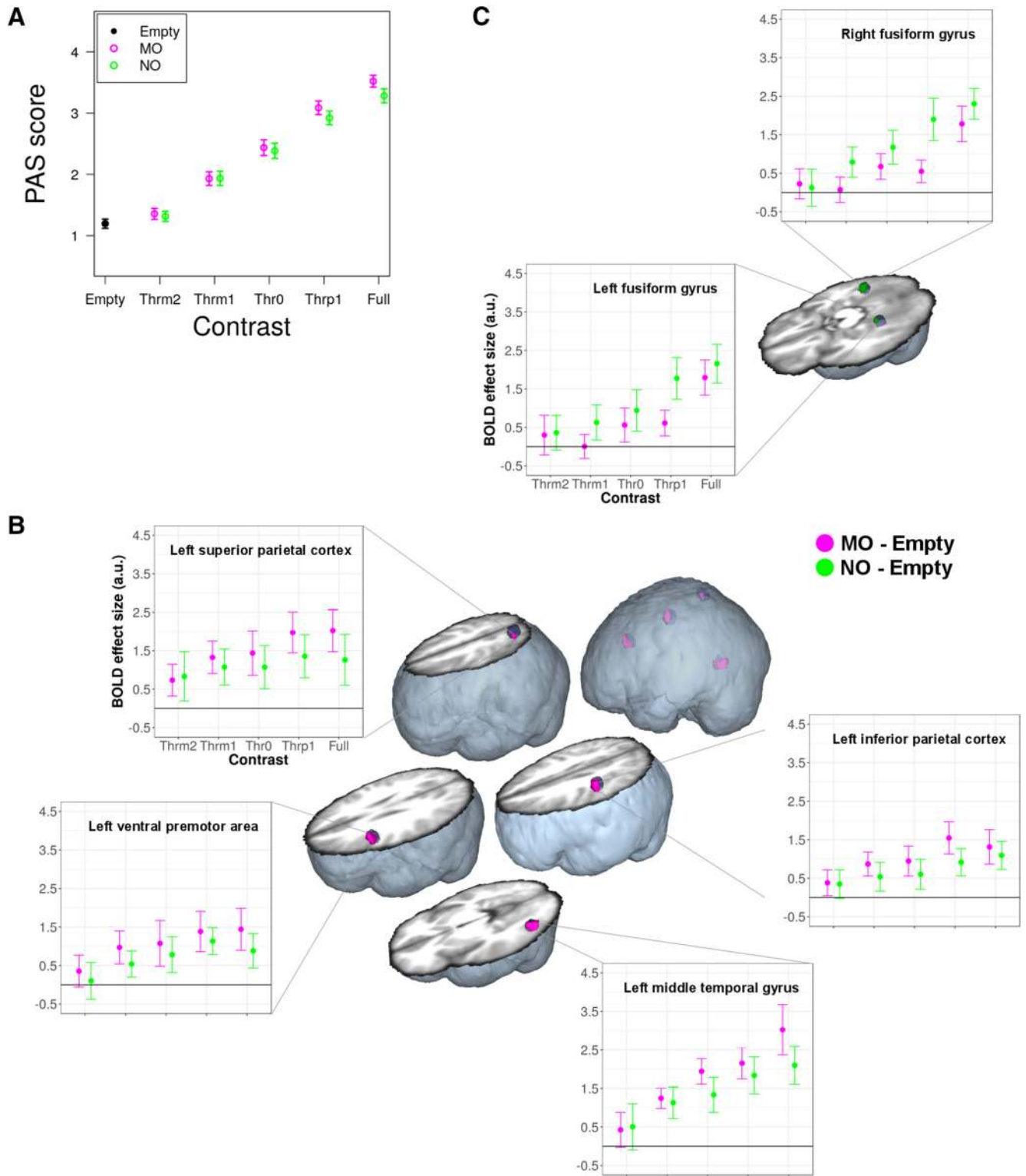
Figure 2. BOLD as a function of contrast. **A**, Average (n = 24) behavioral PAS ratings for MO and NO as a function of image contrast level. Vertical bars indicate 95% confidence intervals. **B**, Subliminal MO-specific brain activation in the OAS and in the left lateral middle temporal gyrus as a function of contrast (n = 24). Brain activations (corrected p < 0.05; purple) are overlaid on the small volumes-of-interest (blue spheres) and displayed on a volumetric rendering of the average anatomical image of all participants. Dot-plots indicate average BOLD responses across all significant voxels in the activation cluster. Vertical bars indicate 95% confidence intervals. **C**, Subliminal NO-specific brain activation (green; all other conventions are identical to **B**) as a function of contrast (n = 24, corrected p < 0.05), with significant effects in the left and right fusiform gyri.

Declared significance threshold for fMRI univariate statistical analyses. For all the reported fMRI analyses, the significance threshold was declared at peak level $p < 0.05$, using a small volume familywise Error type correction for multiple comparisons, with spherical small volumes of 6 mm radius centered on the coordinates of interest (Table 1).

MVPA of fMRI data. MVPA was performed using the PyMVPA 2.6.1 toolbox (www.pymvpa.org, RRID:SCR_006099) running under Python 2.7.13. The analysis was performed on spmT map images (Misaki et al., 2010), obtained by re-estimating the SPM12 univariate first-level analyses on preprocessed but spatially unsmoothed fMRI data. No Z-scoring,

or averaging were applied within the PyMVPA toolbox. The analysis was restricted to voxels within 12 mm radius spheres centered on the coordinates of interest (Table 1), and with gray matter tissue probability >0.1.

We trained a linear support vector machine classifier to distinguish the MO from the NO spmT maps, based on a leave-one-subject-out cross-validation procedure, analogous to a second-level, random-effects analysis (Ghio et al., 2016). More specifically, we performed a searchlight analysis (Kriegeskorte et al., 2006) with 4-mm-radius spheres, and for each sphere we calculated the mean classification accuracy across leave-one-subject-out folds, together with the confusion matrix of predicted against actual classes.

The significance of the classification accuracies was determined through a Monte Carlo procedure, by randomly permuting the MO and NO spmT map labels in each sphere 1000 times (Stelzer et al., 2013), and by then comparing the actual classification accuracy against the random permutation distribution with a declared a $p < 0.005$ threshold.

We report the mean classification accuracies and the corresponding confusion matrices for the significant searchlight spheres, resulting from the analysis of 6 spmT map sets. Three sets entered a MVPA as a function of contrast: (1) across all contrast levels (Thrm2, Thrm1, Thr0, Thrp1, Full), (2) across levels below perceptual threshold (Thrm2, Thrm1), and (3) across levels above perceptual threshold (Thrp1, Full). Three sets entered a MVPA as a function of PAS ratings: (1) across all PAS scores [PAS(1,2), PAS(3,4)], (2) across PAS scores 1 or 2 [PAS(1,2)], and (3) across PAS scores 3 or 4 [PAS(3,4)].

All the included spmT maps incorporated the Empty baseline subtraction (e.g., MOThrm2 − Empty).

Results

Behavioral data collected during fMRI

By analyzing the PAS behavioral responses during fMRI, we made sure that the image Contrast level significantly modulated the level of subjective awareness. A generalized linear mixed model provided evidence that contrast ($\chi^2_{(4)} = 233.94, p < 2.2 \times 10^{-16}$), and not manipulability ($\chi^2_{(1)} = 0.38, p = 0.537$), was a significant predictor of PAS ratings. The Contrast × Manipulability interaction was not significant ($\chi^2_{(4)} = 0.98, p = 0.913$): for both MO and NO, Contrast increase produced a nearly linear increase of subjective awareness (Fig. 2A). Contrasts below the perceptual threshold yielded low to minimal PAS scores, whereas those above the perceptual threshold yielded high to maximal PAS scores.

Main effect of manipulability

As for neural activations induced by CFS, we first evaluated the main effect of manipulability to verify that MO induced higher than NO response amplitudes in the OAS. We indeed found stronger activation for MO versus NO in the ventral premotor, inferior parietal, and superior parietal cortices. Outside the OAS, in brain regions specifically involved in object identification, the lateral middle temporal gyrus also displayed stronger activation for MO versus NO, whereas the reverse effect (NO > MO) was found in the left and right fusiform gyri (Table 2). We found comparable effects of manipulability (Table 3) also when considering only the contrast levels above perceptual threshold (Thrp1, Full), that is under perceptual conditions that genuinely reflect the visible visual features of each object category.

Subliminal fMRI activation as a function of contrast

Crucially, we sought for evidence that, also below perceptual threshold, MO induced stronger than NO activation in the OAS. To this aim, we tested whether the levels of contrast modulated OAS activation following either a subliminal (i.e., activation both above and below perceptual threshold), a step (i.e., activation only above perceptual threshold), or a linear (i.e., gradual activa-

Table 2. Main effect of manipulability

Brain region	Voxels	p value	$Z_{(1,230)}$	MNI coordinates, mm		
				x	y	z
MO > NO						
L ventral premotor cortex	17	0.016	3.03	−50	8	28
L inferior parietal cortex	22	0.007	3.33	−48	−28	44
L superior parietal cortex	4	0.044	2.62	−28	−60	60
L lateral middle temporal gyrus	39	0.004	3.48	−50	−70	−4
NO > MO						
L fusiform gyrus	18	4.1×10^{-4}	4.15	−26	−42	−12
R fusiform gyrus	21	8.5×10^{-9}	6.26	32	−46	−8

MO-specific (MO > NO) and NO-specific (NO > MO) brain activation ($n = 24$). All reported effects passed a peak-level small volume familywise error $p < 0.05$ correction. L, Left; R, right.

Table 3. Simple effect of manipulability for image contrast levels above perceptual threshold (Thrp1, Full)

Brain region	Voxels	p value	$Z_{(1,230)}$	MNI coordinates, mm		
				x	y	z
MO > NO						
L ventral premotor cortex	36	0.074*	2.39	−50	8	28
L inferior parietal cortex	11	0.021	2.93	−50	−30	40
L superior parietal cortex	4	0.022	2.90	−28	−60	60
L lateral middle temporal gyrus	23	0.002	3.72	−50	−70	4
NO > MO						
L fusiform gyrus	22	0.001	3.94	−24	−44	−12
R fusiform gyrus	22	4.5×10^{-8}	5.99	32	−46	−8

MO-specific (MO > NO) and NO-specific (NO > MO) brain activation ($n = 24$). All reported effects passed a peak-level small volume familywise error $p < 0.05$ correction, except for the statistical trend (corrected $p < 0.1$) in the ventral premotor cortex (marked by an asterisk). L, Left; R, right.

tion increase with contrast) BOLD amplitude model (Fig. 1C). The strongest evidence indicated that MO-specific processing conformed to a subliminal model, with significant (small volume familywise error type correction for multiple comparisons for all reported P values) effects in the ventral premotor cortex ($p = 0.008, Z_{(1,23)} = 3.36$, 30 voxels, $x = −50, y = 8, z = 28$), inferior parietal cortex ($p = 0.008, Z_{(1,23)} = 3.35$, 23 voxels, $x = −48, y = −28, z = 44$), and superior parietal cortex ($p = 0.040, Z_{(1,23)} = 2.73$, 5 voxels, $x = −28, y = −60, z = 60$). MO-specific subliminal processing also extended into the lateral middle temporal gyrus ($p = 0.004, Z_{(1,23)} = 3.59$, 37 voxels, $x = −50, y = −68, z = −4$; Fig. 2B). NO-specific subliminal activation was found in the left ($p = 0.032, Z_{(1,23)} = 2.82$, 7 voxels, $x = −26, y = −42, z = −12$) and right ($p = 0.001, Z_{(1,23)} = 4.07$, 18 voxels, $x = 32, y = −46, z = −8$) fusiform gyri (Fig. 2C).

In the OAS, there was no evidence of MO-specific step BOLD modulation. NO-specific step BOLD modulation was found in the bilateral fusiform gyri ($p = 0.047, Z_{(1,23)} = 2.67$, 27 voxels, $x = −26, y = −46, z = −12$; $p = 0.004, Z_{(1,23)} = 3.62$, 22 voxels, $x = 30, y = −48, z = −8$), with a concomitant linear activation profile in the right fusiform gyrus ($p = 0.001, Z_{(1,23)} = 3.89$, 12 voxels, $x = 30, y = −48, z = −8$). Evidence of MO-specific linear modulation in the OAS was limited to the superior parietal cortex ($p = 0.026, Z_{(1,23)} = 2.92$, 2 voxels, $x = −28, y = −62, z = 60$), but also extended outside the OAS, in the lateral middle temporal gyrus ($p = 0.016, Z_{(1,23)} = 3.10$, 16 voxels, $x = −50, y = −70, z = −4$). These two brain regions thus presented a concomitant subliminal and linear activation profile as a function of contrast, indicating significant activation both below and above perceptual threshold, with relatively higher response amplitudes as the contrast level increased.
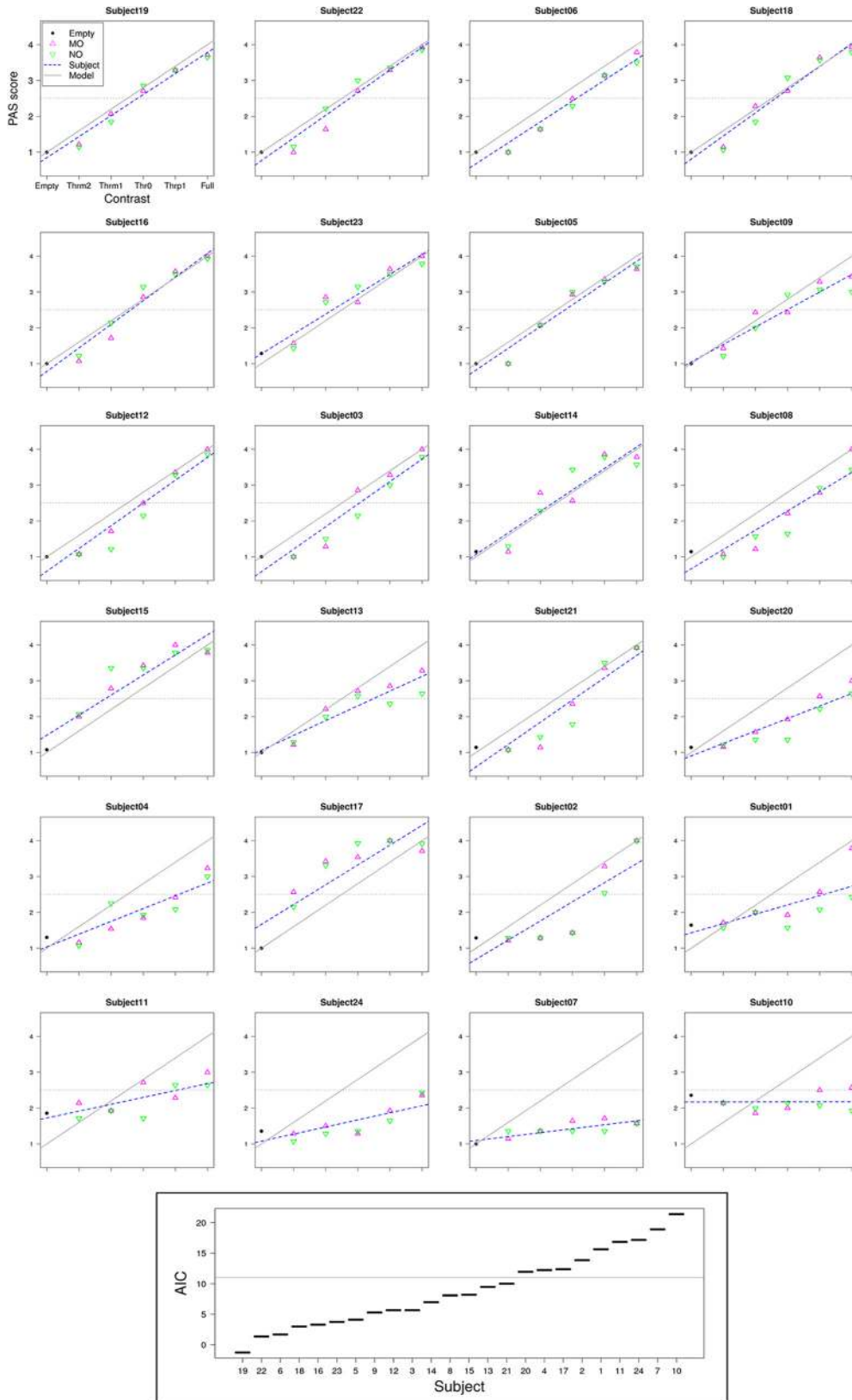
Figure 3. Selection of participants for the BOLD analysis as a function of PAS. The subjects were ranked according to the Akaike information criterion (AIC), obtained by maximum likelihood estimation of the fit of the individual Contrast-to-PAS linear function (blue dashed line) to a Contrast-to-PAS linear model function (gray line). The subsample was defined by selecting the best-ranked subjects, until AIC discontinuity from the n-ranked to the $n+1$-ranked subject (horizontal line in bottom inset). Subjects 14, 15, and 23 were excluded from the subsample because they presented higher than half-maximum (horizontal dashed line) PAS scores at contrast level Thrm1, indicating that a relatively high proportion of stimuli below perceptual threshold were actually visible to these subjects. This left the subsample with 12 subjects. This subsample of subjects presented a comparable modulation of behavioral subjective awareness by image contrast as the whole group (Fig. 4A), as well as comparable activation as a function of contrast both above and below perceptual threshold.
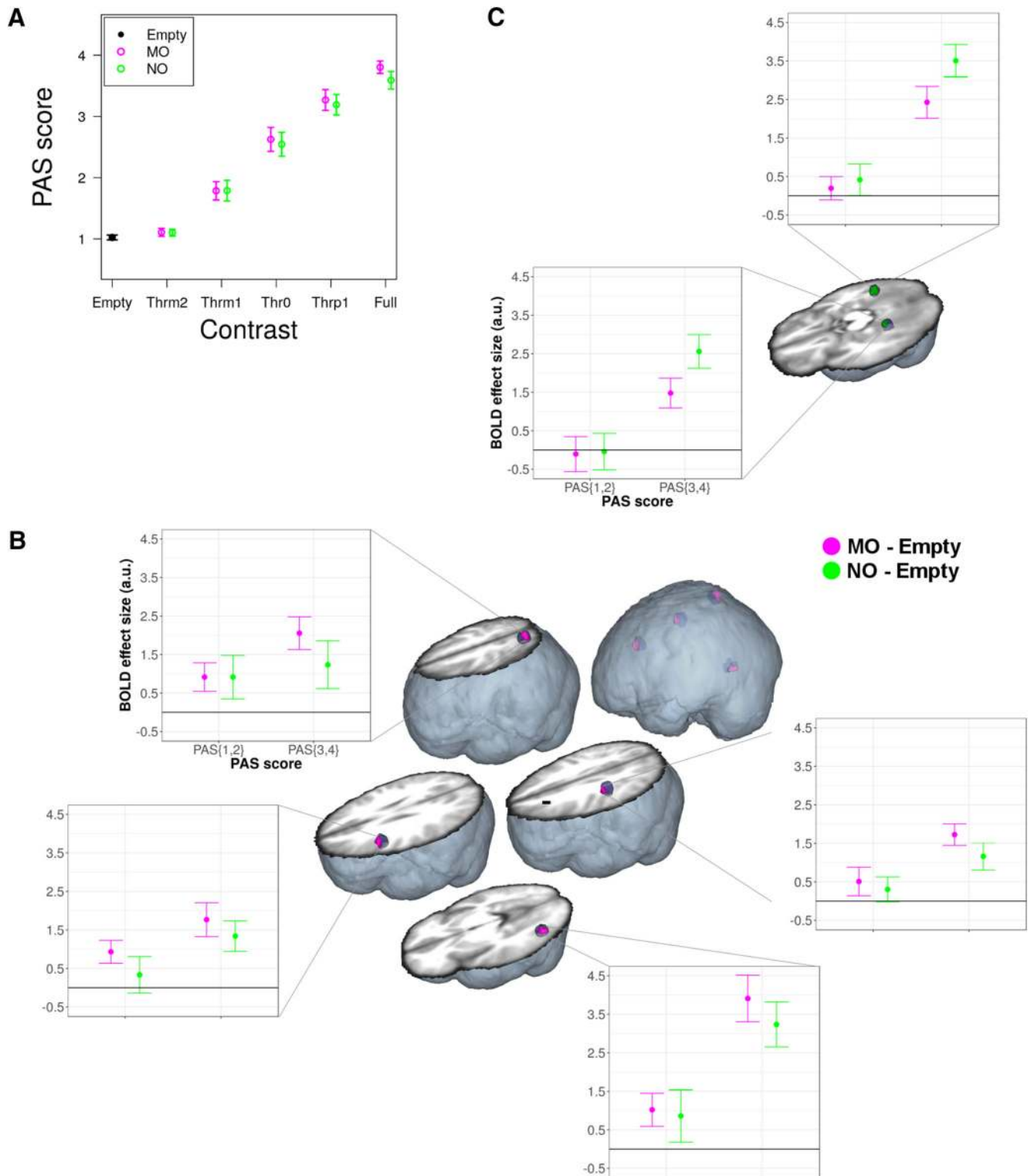
Figure 4. BOLD as a function of PAS. All conventions are identical to Figure 2. **A**, Average ($n = 12$) behavioral PAS ratings for MO and NO as a function of image contrast level in the subsample of 12 subjects included in the BOLD analysis as a function of PAS. Vertical bars indicate 95% confidence intervals. We found that contrast ($\chi^2_{(4)} = 248.51, p < 2.2 \times 10^{-16}$), and not manipulability ($\chi^2_{(1)} = 0.15, p = 0.699$), was a significant predictor of PAS ratings. The Contrast $\times$ Manipulability interaction was not significant ($\chi^2_{(4)} = 0.46, p = 0.977$). **B**, Subliminal MO-specific brain activation in the OAS and in the left lateral middle temporal gyrus as a function of PAS ratings ($n = 12$, corrected $p < 0.05$). PAS(1, 2) = level of the PAS score factor corresponding to CFS trials in which the reported PAS score was either 1 or 2; PAS(3,4) = level for trials with reported PAS score 3 or 4. **C**, Subliminal NO-specific brain activation as a function of PAS ratings ($n = 12$, corrected $p < 0.05$), with significant effects in the left and right fusiform gyri.

Subliminal fMRI activation as a function of PAS

To gain conclusive evidence that MO specifically activated the OAS, not only above but also under subliminal perceptual conditions, we further analyzed BOLD responses as a function of PAS ratings. This allowed us to test whether the presence of a MO stimulus elicited specific responses in the OAS also in the absence of subjective awareness, independently of image contrast. We restricted this analysis to only those subjects that produced com-
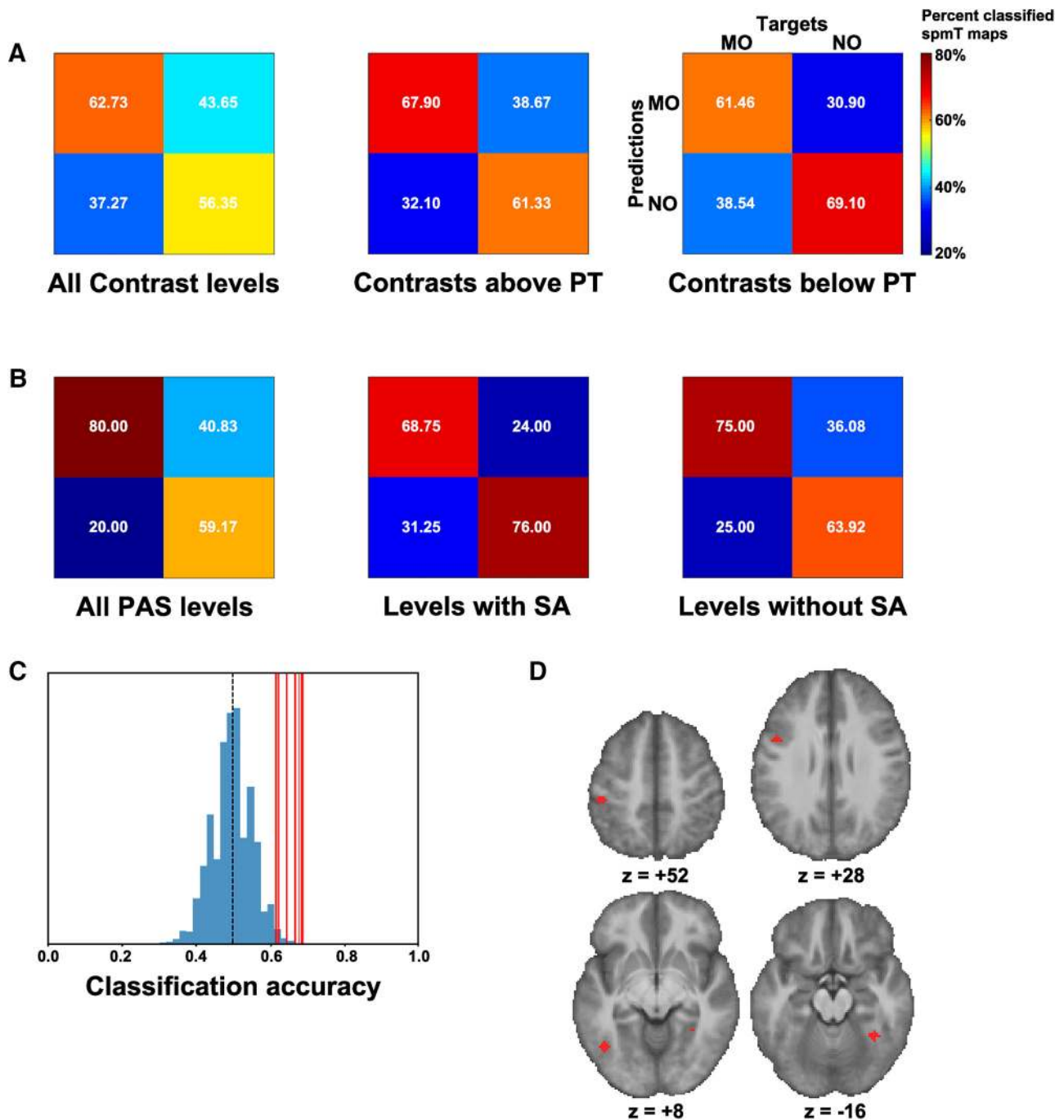
Figure 5. Multivariate pattern analysis. *A*, MVPA as a function of contrast: confusion matrices reporting the means of the classified MO/NO spmT maps across the significant ($p < 0.005$, against 1000 permutations) searchlight spheres, expressed as percentage values, for the analysis of all contrast levels (left), all levels above perceptual threshold (middle), and all levels below perceptual threshold (right; with fully labeled matrix structure, which is the same for all matrices in *A* and *B*). *B*, MVPA as a function of PAS ratings: map classification means across the significant searchlight spheres, expressed as percentage values, for the analysis of all PAS levels (left), just the PAS levels indicating presence of subjective awareness (middle), and just the PAS levels indicating absence of subjective awareness (right). *C*, MVPA as a function of contrast, all levels below perceptual threshold: actual classification accuracies for the significant searchlights (red lines), against the accuracy distribution of 1000 random permutations (blue histogram). The black dashed line indicates the chance classification level. *D*, MVPA as a function of contrast, all levels below perceptual threshold: anatomical location of the significant searchlights, in the ventral premotor cortex, inferior parietal cortex, lateral middle temporal gyrus, and right fusiform gyrus (Table 4).

parable response frequencies across all PAS levels (Figs. 3, 4*A*). The strongest evidence indicated that, as a function of PAS ratings, MO specifically activated the OAS conforming to a subliminal BOLD amplitude model (i.e., activation both with and without subjective awareness; Fig. 1*C*). Significant subliminal effects were located in the ventral premotor cortex ($p = 0.013$, pseudo $t = 3.28$, 13 voxels, $x = -50$, $y = 12$, $z = 32$), inferior parietal cortex ($p = 0.032$, pseudo $t = 2.92$, 8 voxels, $x = -48$,

$y = -28$, $z = 44$), and in the superior parietal cortex ($p = 0.017$, pseudo $t = 3.01$, 10 voxels, $x = -22$, $y = -66$, $z = 60$). The lateral middle temporal gyrus ($p = 0.022$, pseudo $t = 2.89$, 12 voxels, $x = -46$, $y = -66$, $z = -4$) also presented a subliminal response (Fig. 4*B*). NO-specific subliminal activation was found in the left ($p = 0.016$, pseudo $t = 3.30$, 10 voxels, $x = -30$, $y = -42$, $z = -12$) and right ($p = 0.003$, pseudo $t = 5.01$, 18 voxels, $x = 30$, $y = -50$, $z = -8$) fusiform gyri (Fig. 4*C*).

Table 4. Number and anatomical location of the significant searchlights in the MVPAs as a function of either contrast or PAS ratings, with respect to the set of regions-of-interest, based on the meta-analysis on tool-related cognition by Ishibashi et al. (2016)

	MVPA by contrast			MVPA by PAS ratings		
	All levels	Below perceptual threshold	Above perceptual threshold	All levels	Without subjective awareness	With subjective awareness
No. of significant searchlights (p < 0.005, against 1000 permutations)	63	6	79	5	3	8
L ventral premotor cortex	Yes	Yes	—	Yes	—	—
L dorsal premotor cortex	—	—	—	—	Yes	—
L inferior parietal cortex	Yes	Yes	Yes	—	Yes	—
L superior parietal cortex	Yes	—	—	—	—	Yes
L lateral middle temporal gyrus	Yes	Yes	Yes	—	Yes	Yes
L fusiform gyrus	Yes	—	Yes	Yes	—	Yes
R fusiform gyrus	Yes	Yes	Yes	Yes	—	Yes

Concomitantly to a subliminal BOLD modulation, we also found evidence of a step BOLD modulation in the inferior parietal cortex ($p = 0.042$, pseudo $t = 2.72$, 1 voxel, $x = -44$, $y = -30$, $z = 48$), superior parietal cortex ($p = 0.003$, pseudo $t = 3.80$, 19 voxels, $x = -26$, $y = -64$, $z = 60$), and in the lateral middle temporal gyrus ($p = 0.032$, pseudo $t = 2.72$, 11 voxels, $x = -44$, $y = -68$, $z = -4$). This indicates significant activation both with and without subjective awareness, compared with the Empty baseline, but relatively stronger activation with than without subjective awareness. NO-specific step BOLD modulation was found in the left ($p = 0.001$, pseudo $t = 4.35$, 38 voxels, $x = -28$, $y = -46$, $z = -12$) and right ($p = 2.0 \times 10^{-4}$, pseudo $t = 4.75$, 19 voxels, $x = 30$, $y = -50$, $z = -8$) fusiform gyri.

Multivariate classification of fMRI activation patterns
To evaluate whether the MO versus NO activation differences, as resulting from the univariate fMRI analyses, pointed to clearly identifiable object-type-specific neural coding in the OAS, such that a supporting vector machine classifier would be able to tell MO from NO activation maps, we also ran a searchlight MVPA on the same fMRI data.

In the analysis as a function of contrast (Fig. 5A), the MVPA classifier distinguished MO and NO significantly above chance, whether we considered all Contrast levels (mean classification accuracy = 59.5%), just those above perceptual threshold (mean accuracy = 64.6%), or most importantly, just the contrast levels below perceptual threshold (mean accuracy = 65.3%). Also in the analysis as a function of PAS ratings (Fig. 5B), MO and NO were correctly classified significantly above chance, whether we considered all PAS levels (mean accuracy = 69.6%), just those indicating presence of subjective awareness (mean accuracy = 72.4%), or, most importantly, just the PAS levels indicating absence of subjective awareness (mean accuracy = 69.4%).

In all these classification analyses, the significant searchlights (Fig. 5C) were located in subsets of the anatomical regions of interest (Table 1) that spanned both the dorsal and ventral visuomotor pathways (Fig. 5D; Table 4).

Discussion
Resting upon unambiguous behavioral evidence of an absence of subjective awareness for object stimuli presented with image contrasts below perceptual threshold, our fMRI results indicate that action-related properties of MO are capable of triggering a visuo-

motor functional response, even under unaware processing conditions. Consistently across all the different univariate analyses of BOLD signal that we performed, whether considering picture contrast levels below perceptual threshold, as imposed by the experimenters, or the absence of subjective awareness, based on the participants' responses, the subliminal MO-specific activation extended to the left-lateralized premotor-parietal OAS and, outside the OAS, in the lateral posterior temporal cortex. This left-hemispheric premotor-parietal-temporal network was also consistently implicated in the multivariate searchlight decoding of MO- versus NO-specific activation patterns, again both when considering contrast levels below perceptual threshold and the absence of subjective awareness. Whereas numerous studies have previously found activation in this left-hemispheric premotor-parietal-temporal network for visible manipulable objects (Chao and Martin, 2000; Grèzes et al., 2003; Canessa et al., 2008; Caspers et al., 2010; Macdonald and Culham, 2015; Ishibashi et al., 2016), our study clearly demonstrates that comparable functional effects also occur under unaware perceptual conditions.

Among the brain regions displaying either MO-specific or NO-specific subliminal BOLD activation, those located more ventrally (i.e., fusiform gyri and lateral occipitotemporal cortex) showed the highest degree of concomitant linearity, with relatively greater activation as contrast and subjective awareness increased. More dorsally, the premotor-parietal cortices instead displayed a more stable activation level across image contrasts, below and above perceptual threshold. All things considered, the single most important observation with respect to our hypotheses is that even the MO-specific brain regions displaying a linearly increasing activation, at the same time presented a significant activation below the perceptual threshold, as indicated by the concomitant subliminal response profile. This pattern of results clearly differs from an alternative possibility for which we found no evidence in our data, namely, linearly increasing activation, with significant activation only above and not below perceptual threshold. In contrast, radically distinct (i.e., all or none) fMRI response profiles as a function of awareness in posterior dorsal versus ventral areas were observed for tool pictures in previous CFS studies, although with conflicting results, possibly due to methodological factors (e.g., mask textures) differing among studies (Ludwig and Hesselmann, 2015). A fMRI study (Fang and He, 2005) showed tool-specific activation to be restricted in the dorsal visual stream, with no relevant contribution of ventral visual stream brain regions. Behavioral CFS studies were largely supportive of these findings, providing evidence of tool-selective responses compatible with an engagement of dorsal visual stream brain regions (Almeida et al., 2008, 2010). Other studies did not find any activation of the dorsal visual stream for unawarely processed tool stimuli (Hesselmann and Malach, 2011; Hesselmann et al., 2011; Fogelson et al., 2014; Ludwig et al., 2015, 2016).

It must be noted that all the previously mentioned CFS studies limited their focus to posterior brain regions along the dorsal and ventral visual streams, compatible with a purely visual account of decoding the action properties of manipulable objects (Goodale and Milner, 1992; Milner and Goodale, 2008). However, the encoding, storage, and retrieval of manipulable object knowledge has been shown to depend crucially on the functional involvement of more anterior brain regions along the dorsal pathway, notably the premotor cortex (Johnson-Frey, 2004; Lewis, 2006; Caspers et al., 2010; Ishibashi et al., 2016). Canonical neurons in premotor-parietal circuits constitute a fundamental neurophysiological correlate of the visuomotor transformation of manipulable object perceptual information (Gallese et al., 1996; Murata

et al., 1997). This evidence of an involvement of the premotor cortex prompts a visuomotor account, as opposed to a purely visual account, of manipulable object representation (Buxbaum and Kalénine, 2010). Accordingly, we show here for the first time that both ventral and dorsal visual streams, extending into anterior parietal and premotor regions, that is, into the entire OAS, support unaware processing of visual MO information. The ventral and the premotor-parietal streams have been shown to code for the manipulability and functional properties of tools in semantic memory (Canessa et al., 2008). The issue of semantic memory is relevant in the context of the present study, because the visual presentation of an object picture under CFS, followed by a subjective rating of perceptual awareness, enforced object identification at the conceptual-semantic level. There were no overt task assignments that implied imagining or carrying out actions toward depicted manipulable objects. This, at least in principle, opens the possibility that the visuomotor coding of MO-specific features such as manipulability and affordance becomes integrated into the conceptual-semantic representation of the perceived manipulable objects. Our results may therefore be compatible with embodied and grounded cognition theories of conceptual knowledge, which postulate the participation of perceptual and motor cortices in the semantic representation of manipulable objects (Kiefer and Pulvermüller, 2012; Lambon Ralph et al., 2017). Though our data cannot advocate for one particular theoretical position along the spectrum from secondary or weak to strong embodiment (Binder and Desai, 2011; Meteyard et al., 2012), they are consistent with the general view that a detailed conceptual representation extends over a distributed brain system comprising levels or nodes that encode the kind of experiential information relevant for the represented entity (Binder and Desai, 2011; Kiefer and Barsalou, 2012). In keeping with this view, we propose to interpret our finding of MO-specific ventral and dorsal stream activation as suggestive of visuomotor coding of tool-related features that contributes in forming the conceptual knowledge of the depicted tool objects, even at subliminal levels.

In this study, the results of the univariate analysis, and to a large extent also those of the multivariate analysis, implicate the ventral premotor rather than the dorsal premotor cortex in the aware and unaware processing of MO. Among the OAS regions, as defined based on the meta-analysis by Ishibashi et al. (2016), the left dorsal premotor cortex was the one that showed the less responsivity, if any, to tool pictures. One possibility for this lack of response is that the left dorsal premotor cortex, unlike the other OAS regions, is exclusively involved in a dorso-dorsal visuomotor stream coding for structural action affordances during online hand-object interactions, as opposed to a ventrodorsal stream coding off-line object manipulability (Buxbaum and Kalénine, 2010; Sakreida et al., 2016). An alternative possibility is the dorsal premotor cortex's role in internally generated action sequences, as opposed to visually cued object target coding, the latter rather involving the ventral premotor cortex (Ohbayashi et al., 2016).

A possible concern might be that the stronger OAS response that we observed for MO, both with and without awareness, is not due to their specific visual characteristics of manipulability and affordance, but rather to irrelevant perceptual dimensions, such as visual salience or object shape. Previous behavioral studies using CFS have cast doubts on whether unaware processing in the dorsal visual stream may be indeed due to the manipulability of tool objects, or simply to their typical elongated shape. Comparable effects were indeed found for elongated entities of other

semantic categories, such as vegetables, geometrical shapes, or animals (Sakuraba et al., 2012; Hesselmann et al., 2016). However, neuroimaging studies using fully visible stimuli have demonstrated that, although shape elongation is a primary factor in determining dorsal visual stream activation responses (Fabbri et al., 2016), tool-specific activation in dorsal stream regions occur even after controlling for elongation (Macdonald and Culham, 2015; Chen et al., 2017). Building upon such subtle experimental disentanglement of perceptual dimensions, we took care to carefully match the elongation shape of our MO and NO picture stimuli. Visual complexity was also carefully matched. Altogether, these considerations make the caveat on irrelevant perceptual dimension quite unlikely. Also, the fact that, outside the OAS, NO pictures elicited patterns of increased BOLD activation compared with MO, provides evidence of a functional double dissociation that is not compatible with a simple explanation based on a putative greater visual salience for MO than for NO pictures. NO-specific BOLD responses were found in the fusiform gyri, both with and without perceptual awareness, and this finding is consistent with previous studies that also showed the involvement of this brain region in the representation of non-manipulable inanimate objects (Ishai et al., 2000; Saccuman et al., 2006).

Recent evidence has demonstrated that visual objects that are not consciously perceived give rise to a neurophysiological response signature that is indistinguishable from that generated by consciously perceived objects (Fahrenfort et al., 2017). Our results confirm and extend these findings, in that they provide crucial evidence of the intimate neural coupling between visual perception and motor representation that underlies manipulable object processing, endowing the brain with an efficient mechanism for monitoring and planning actions and reactions to external world's stimuli, even if these stimuli momentarily escape awareness.

References

Almeida J, Mahon BZ, Nakayama K, Caramazza A (2008) Unconscious processing dissociates along categorical lines. Proc Natl Acad Sci U S A 105: 15214–15218. CrossRef Medline

Almeida J, Mahon BZ, Caramazza A (2010) The role of the dorsal visual processing stream in tool identification. Psychol Sci 21:772–778. CrossRef Medline

Binder JR, Desai RH (2011) The neurobiology of semantic memory. Trends Cogn Sci 15:527–536. CrossRef Medline

Bracci S, Cavina-Pratesi C, Ietswaart M, Caramazza A, Peelen MV (2012) Closely overlapping responses to tools and hands in left lateral occipitotemporal cortex. J Neurophysiol 107:1443–1456. CrossRef Medline

Brodeur MB, Dionne-Dostie E, Montreuil T, Lepage M (2010) The bank of standardized stimuli (BOSS), a new set of 480 normative photos of objects to be used as visual stimuli in cognitive research. PLoS One 5:e10773. CrossRef Medline

Brodeur MB, Guérard K, Bouras M (2014) Bank of standardized stimuli (BOSS) phase II: 930 new normative photos. PLoS One 9:e106953. CrossRef Medline

Buxbaum LJ, Kalénine S (2010) Action knowledge, visuomotor activation, and embodiment in the two action systems. Ann N Y Acad Sci 1191:201–218. CrossRef Medline

Canessa N, Borgo F, Cappa SF, Perani D, Falini A, Buccino G, Tettamanti M, Shallice T (2008) The different neural correlates of action and functional knowledge in semantic memory: an FMRI study. Cereb Cortex 18:740–751. CrossRef Medline

Carmel D, Arcaro M, Kastner S, Hasson U (2010) How to create and use binocular rivalry. J Vis Exp 45:e2030. CrossRef Medline

Caspers S, Zilles K, Laird AR, Eickhoff SB (2010) ALE meta-analysis of action observation and imitation in the human brain. Neuroimage 50:1148–1167. CrossRef Medline

Chao LL, Martin A (2000) Representation of manipulable man-made objects in the dorsal stream. Neuroimage 12:478–484. CrossRef Medline

Chao LL, Haxby JV, Martin A (1999) Attribute-based neural substrates in temporal cortex for perceiving and knowing about objects. Nat Neurosci 2:913–919. CrossRef Medline

Chen J, Snow JC, Culham JC, Goodale MA (2017) What Role does "elongation" play in "tool-specific" activation and connectivity in the dorsal and ventral visual streams? Cereb Cortex. Advance online publication. doi: 10.1093/cercor/bhx017. Medline

Cul A, Baillet S, Dehaene S (2007) Brain dynamics underlying the nonlinear threshold for access to consciousness. PLoS Biol 5:e260. CrossRef Medline

Fabbri S, Stubbs KM, Cusack R, Culham JC (2016) Disentangling representations of object and grasp properties in the human brain. J Neurosci 36:7648–7662. CrossRef Medline

Fahrenfort JJ, van Leeuwen J, Olivers CN, Hogendoorn H (2017) Perceptual integration without conscious access. Proc Natl Acad Sci U S A 114:3744–3749. CrossRef Medline

Fang F, He S (2005) Cortical responses to invisible objects in the human dorsal and ventral pathways. Nat Neurosci 8:1380–1385. CrossRef Medline

Fogelson SV, Kohler PJ, Miller KJ, Granger R, Tse PU (2014) Unconscious neural processing differs with method used to render stimuli invisible. Front Psychol 5:601. CrossRef Medline

Gallese V, Fadiga L, Fogassi L, Rizzolatti G (1996) Action recognition in the premotor cortex. Brain 119:593–609. CrossRef Medline

Ghio M, Vaghi MMS, Perani D, Tettamanti M (2016) Decoding the neural representation of fine-grained conceptual categories. Neuroimage 132:93–103. CrossRef Medline

Goodale MA, Milner AD (1992) Separate visual pathways for perception and action. Trends Neurosci 15:20–25. CrossRef Medline

Grèzes J, Armony JL, Rowe J, Passingham R (2003) Activations related to "mirror" and "canonical" neurones in the human brain: an fMRI study. Neuroimage 18:928–937. CrossRef Medline

Hesselmann G, Malach R (2011) The link between fMRI-BOLD activation and perceptual awareness is "stream-invariant" in the human visual system. Cereb Cortex 21:2829–2837. CrossRef Medline

Hesselmann G, Hebart M, Malach R (2011) Differential BOLD activity associated with subjective and objective reports during "blindsight" in normal observers. J Neurosci 31:12936–12944. CrossRef Medline

Hesselmann G, Darcy N, Ludwig K, Sterzer P (2016) Priming in a shape task but not in a category task under continuous flash suppression. J Vis 16(13):17 1–17. CrossRef Medline

Ishai A, Ungerleider LG, Haxby JV (2000) Distributed neural systems for the generation of visual images. Neuron 28:979–990. CrossRef Medline

Ishibashi R, Pobric G, Saito S, Lambon Ralph MA (2016) The neural network for tool-related cognition: an activation likelihood estimation meta-analysis of 70 neuroimaging contrasts. Cogn Neuropsychol 33:241–256. CrossRef Medline

Johnson-Frey SH (2004) The neural bases of complex tool use in humans. Trends Cogn Sci 8:71–78. CrossRef Medline

Kiefer M, Barsalou LW (2012) Grounding the human conceptual system in perception, action, and internal states. In: Tutorials in action science (Prinz W, Beisert M, Herwig A, eds). Cambridge, MA: MIT.

Kiefer M, Pulvermüller F (2012) Conceptual representations in mind and brain: theoretical developments, current evidence and future directions. Cortex 48:805–825. CrossRef Medline

Kouider S, Dehaene S (2007) Levels of processing during non-conscious perception: a critical review of visual masking. Philos Trans R Soc Lond B Biol Sci 362:857–875. CrossRef Medline

Kriegeskorte N, Goebel R, Bandettini P (2006) Information-based functional brain mapping. Proc Natl Acad Sci U S A 103:3863–3868. CrossRef Medline

Lambon Ralph MA, Jefferies E, Patterson K, Rogers TT (2017) The neural and computational bases of semantic cognition. Nat Rev Neurosci 18:42–55. CrossRef Medline

Lewis JW (2006) Cortical networks related to human use of tools. Neuroscientist 12:211–231. CrossRef Medline

Ludwig K, Hesselmann G (2015) Weighing the evidence for a dorsal processing bias under continuous flash suppression. Conscious Cogn 35:251–259. CrossRef Medline

Ludwig K, Kathmann N, Sterzer P, Hesselmann G (2015) Investigating category- and shape-selective neural processing in ventral and dorsal vi-

sual stream under interocular suppression. Hum Brain Mapp 36:137–149. CrossRef Medline

Ludwig K, Sterzer P, Kathmann N, Hesselmann G (2016) Differential modulation of visual object processing in dorsal and ventral stream by stimulus visibility. Cortex 83:113–123. CrossRef Medline

Macdonald SN, Culham JC (2015) Do human brain areas involved in visuomotor actions show a preference for real tools over visually similar non-tools? Neuropsychologia 77:35–41. CrossRef Medline

Meteyard L, Cuadrado SR, Bahrami B, Vigliocco G (2012) Coming of age: a review of embodiment and the neuroscience of semantics. Cortex 48:788–804. CrossRef Medline

Miles WR (1930) Ocular dominance in human adults. J Gen Psychol 3:412–430. CrossRef

Milner AD, Goodale MA (2008) Two visual systems re-viewed. Neuropsychologia 46:774–785. CrossRef Medline

Misaki M, Kim Y, Bandettini PA, Kriegeskorte N (2010) Comparison of multivariate classifiers and response normalizations for pattern-information fMRI. Neuroimage 53:103–118. CrossRef Medline

Murata A, Fadiga L, Fogassi L, Gallese V, Raos V, Rizzolatti G (1997) Object representation in the ventral premotor cortex (area F5) of the monkey. J Neurophysiol 78:2226–2230. Medline

Nichols TE, Holmes AP (2002) Nonparametric permutation tests for functional neuroimaging: a primer with examples. Hum Brain Mapp 15:1–25. CrossRef Medline

Ohbayashi M, Picard N, Strick PL (2016) Inactivation of the dorsal premotor area disrupts internally generated, but not visually guided, sequential movements. J Neurosci 36:1971–1976. CrossRef Medline

Oldfield RC (1971) The assessment and analysis of handedness: the Edinburgh inventory. Neuropsychologia 9:97–113. CrossRef Medline

Pizer SM, Amburn EP, Austin JD, Cromartie R, Geselowitz A, Greer T, Romeny BTH, Zimmerman JB (1987) Adaptive histogram equalization and its variations. Comput Vis Graph Image Process 39:355–368. CrossRef

R Core Team (2016) A language and environment for statistical computing. R Foundation for Statistical Computing, Vienna, Austria.

Ramsøy TZ, Overgaard M (2004) Introspection and subliminal perception. Phenom Cogn Sci 3:1–23. CrossRef

Saccuman MC, Cappa SF, Bates EA, Arevalo A, Della Rosa P, Danna M, Perani D (2006) The impact of semantic reference on word class: an fMRI study of action and object naming. Neuroimage 32:1865–1878. CrossRef Medline

Sakreida K, Effnert I, Thill S, Menz MM, Jirak D, Eickhoff CR, Ziemke T, Eickhoff SB, Borghi AM, Binkofski F (2016) Affordance processing in segregated parieto-frontal dorsal stream sub-pathways. Neurosci Biobehav Rev 69:89–112. CrossRef Medline

Sakuraba S, Sakai S, Yamanaka M, Yokosawa K, Hirayama K (2012) Does the human dorsal stream really process a category for tools? J Neurosci 32:3949–3953. CrossRef Medline

Salmon JP, McMullen PA, Filliter JH (2010) Norms for two types of manipulability (graspability and functional usage), familiarity, and age of acquisition for 320 photographs of objects. Behav Res Methods 42:82–95. CrossRef Medline

Sandberg K, Timmermans B, Overgaard M, Cleeremans A (2010) Measuring consciousness: is one measure better than the other? Conscious Cogn 19:1069–1078. CrossRef Medline

Stelzer J, Chen Y, Turner R (2013) Statistical inference and multiple testing correction in classification-based multi-voxel pattern analysis (MVPA): random permutations and cluster size control. Neuroimage 65:69–82. CrossRef Medline

Tsuchiya N, Koch C (2005) Continuous flash suppression reduces negative afterimages. Nat Neurosci 8:1096–1101. CrossRef Medline

Whatmough C, Chertkow H, Murtha S, Hanratty K (2002) Dissociable brain regions process object meaning and object structure during picture naming. Neuropsychologia 40:174–186. CrossRef Medline

Wierenga CE, Perlstein WM, Benjamin M, Leonard CM, Rothi LG, Conway T, Cato MA, Gopinath K, Briggs R, Crosson B (2009) Neural substrates of object identification: functional magnetic resonance imaging evidence that category and visual attribute contribute to semantic knowledge. J Int Neuropsychol Soc 15:169–181. CrossRef Medline

Yang E, Brascamp J, Kang MS, Blake R (2014) On the use of continuous flash suppression for the study of visual processing outside of awareness. Front Psychol 5:724. CrossRef Medline